Site-specific characterization of the Asp- and Glu-ADP-ribosylated proteome

Yajie Zhang, Jianqi Wang, Ming Ding & Yonghao Yu

Poly(ADP-ribosyl)ation is catalyzed by a family of enzymes known as PARPs. We describe a method to characterize the human aspartic acid– and glutamic acid–ADP-ribosylated proteome. We identified 1,048 ADP-ribosylation sites on 340 proteins involved in a wide array of nuclear functions; among these were many previously unknown PARP downstream targets whose ADP-ribosylation was sensitive to PARP inhibitor treatment. We also confirmed that iniparib had a negligible effect on PARP activity in intact cells.

Poly(ADP-ribose) (PAR) is a protein post-translational modification that was first documented more than four decades ago[1]. PAR is composed of linear and/or branched repeats of ADP-ribose, up to a length of 200 units (**Fig. 1a**). Poly(ADP-ribosyl)ation (PARylation) often results in a dramatic change in the electrostatic property of the acceptor protein[2]. PAR may also act as a scaffold for recruiting other proteins to modulate the function of the acceptor protein[3]. PARylation is synthesized by a class of enzymes called PAR polymerases (PARPs), of which 17 members have been identified so far[4]. In particular, PARP1 is a nuclear protein that is activated as a result of sensing DNA strand breaks. In response to genotoxic stress, PARP1 is recruited to nicked DNA and is rapidly activated, resulting in the synthesis of a large number of PARylated proteins and initiation of the DNA damage repair mechanisms[3]. Other biological functions of protein PARylation, however, are largely unknown.

Cancer cells with defects in double-strand break (DSB) repair, such as those with mutations in *BRCA1* or *BRCA2*, are reliant on PARP1 activity for genome integrity and undergo unsustainable genetic damage upon PARP1 inhibition[5]. However, recent late-stage clinical trials found no overall survival benefit from treatment with PARP inhibitors in patients with triple-negative breast cancer[6]. These setbacks underscore that the exact role of PARP in oncogenesis and tumor maintenance is poorly understood.

Protein domains that recognize PAR have been used to capture PARylated proteins for their subsequent identification[7]. However, pinpointing the site of ADP-ribosylation poses a crucial challenge for mass spectrometry. PARylation is a heterogeneous modification, precluding the use of conventional database search approaches for spectrum interpretation. In addition, its pyrophosphate bond, adenine moiety and amino acid side-chain linkage are labile during collision-induced dissociation experiments, yielding neutral-loss fragments instead of sequence-specific ions[8]. As a result, even though a number of amino acids are known to be ADP-ribosylated (aspartic acid, glutamic acid, lysine, arginine, cysteine and asparagine)[9], PARylation sites have been determined for only a few proteins[10].

We sought to develop an approach toward a global characterization of ADP-ribosylation of aspartic acid (Asp-ADP-ribosylation) and glutamic acid (Glu-ADP-ribosylation). We observed increased PARylation in human colorectal carcinoma cells (HCT116) after treatment with 1-methyl-2-nitro-1-nitrosoguanidine (MNNG), a DNA-alkylating agent (**Fig. 1b**). However, the increase was marginal, even though the activity of PARP1 is dramatically upregulated in these conditions[2]. The major cellular activity for degrading PAR comes from PAR glycohydrolase[2] (PARG) (**Supplementary Fig. 1a–c**). To facilitate the characterization of these low-abundance PARylated proteins, we generated PARG-knockdown HCT116 cells using a short hairpin RNA (shRNA) construct, in which we observed a pronounced accumulation of PARylated proteins after treatment with MNNG (**Fig. 1b**) or H_2O_2 (which induces oxidative DNA damage) (**Fig. 1c**). To verify that the increased PARylation was mediated by PARP, we pretreated cells with olaparib, a PARP inhibitor, and observed that PARylation was largely abolished (**Fig. 1c** and **Supplementary Fig. 1d**).

We used boronate-affinity chromatography to isolate ADP-ribosylated peptides. The enrichment is a result of the formation of ester bonds between boron and a 1,2-*cis*-diol moiety within ADP-ribose[11] (**Fig. 1d**). We eluted the ADP-ribosylated peptides by NH_2OH treatment. The ester bond between the first ADP-ribose unit of PAR and the side chain carboxyl group of an aspartic acid and glutamic acid residue is susceptible to NH_2OH attack[12]. However, instead of converting an ADP-ribosylated aspartic acid or glutamic acid back to its unmodified form, which results in the loss of the site information, reaction with NH_2OH generates a hydroxamic acid derivative with an addition of 15.0109 Da (**Fig. 1a**), an increment that can be readily distinguished by mass spectrometry. Notably, transformation of a heterogeneously modified amino acid into a residue with a fixed mass tag greatly facilitates the concurrent identification and site determination of Asp- and Glu-ADP-ribosylated proteins. We confirmed that NH_2OH did not react nonspecifically with free aspartic acid and glutamic acid residues (**Supplementary Fig. 2a** and **Supplementary Results**).

Department of Biochemistry, University of Texas Southwestern Medical Center, Dallas, Texas, USA. Correspondence should be addressed to Y.Y. (yonghao.yu@utsouthwestern.edu).

RECEIVED 13 AUGUST 2012; ACCEPTED 01 JULY 2013; PUBLISHED ONLINE 18 AUGUST 2013; CORRECTED ONLINE 26 AUGUST 2013 (DETAILS ONLINE); DOI:10.1038/NMETH.2603

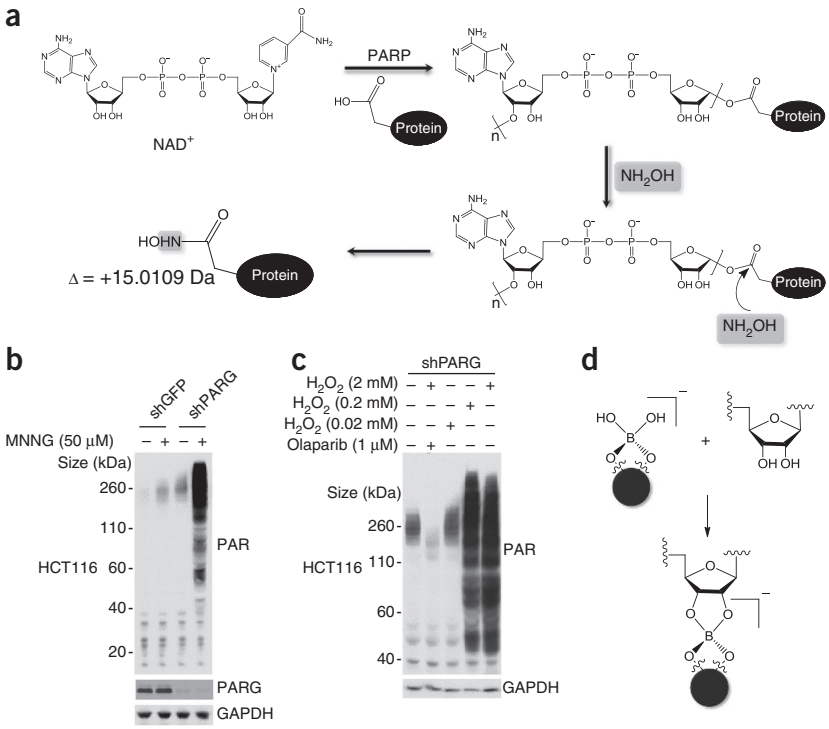

Figure 1 | General scheme for isolation and site determination of protein Asp- and Glu-ADP-ribosylation. (**a**) PARPs use NAD^+ as a cofactor to synthesize PAR. Asp- and Glu-ADP-ribosylation is susceptible to NH_2OH attack, generating a hydroxamic acid derivative. (**b**) PARG-knockdown (shPARG) and control (shGFP) HCT116 cells were treated with 50 μM MNNG for 15 min, and lysates were probed with the antibodies indicated. (**c**) PARG-knockdown cells were treated with various concentrations of H_2O_2, and the resulting lysates were probed with the antibodies indicated. Olaparib was used to block the formation of PARylated proteins. (**d**) Esterification of boron with a 1,2-*cis*-diol moiety within ADP-ribose.

In two experiments, we stimulated PARG-knockdown HCT116 cells with 0.2 mM or 2 mM H_2O_2 and identified 883 Asp- and Glu-ADP-ribosylated peptides from 129 proteins, and 1,129 Asp- and Glu-ADP-ribosylated peptides from 154 proteins, respectively (**Fig. 2a**, **Supplementary Fig. 2** and **Supplementary Tables 1** and **2**). There was substantial overlap, with 102 ADP-ribosylated proteins identified in both experiments (**Fig. 2b**). We confirmed that PARylation did not result from a general apoptosis response (**Supplementary Fig. 2c**). Gene ontology analyses of the modified proteins revealed several enriched biological processes, including chromosome organization ($P = 1.51 \times 10^{-15}$), transcription

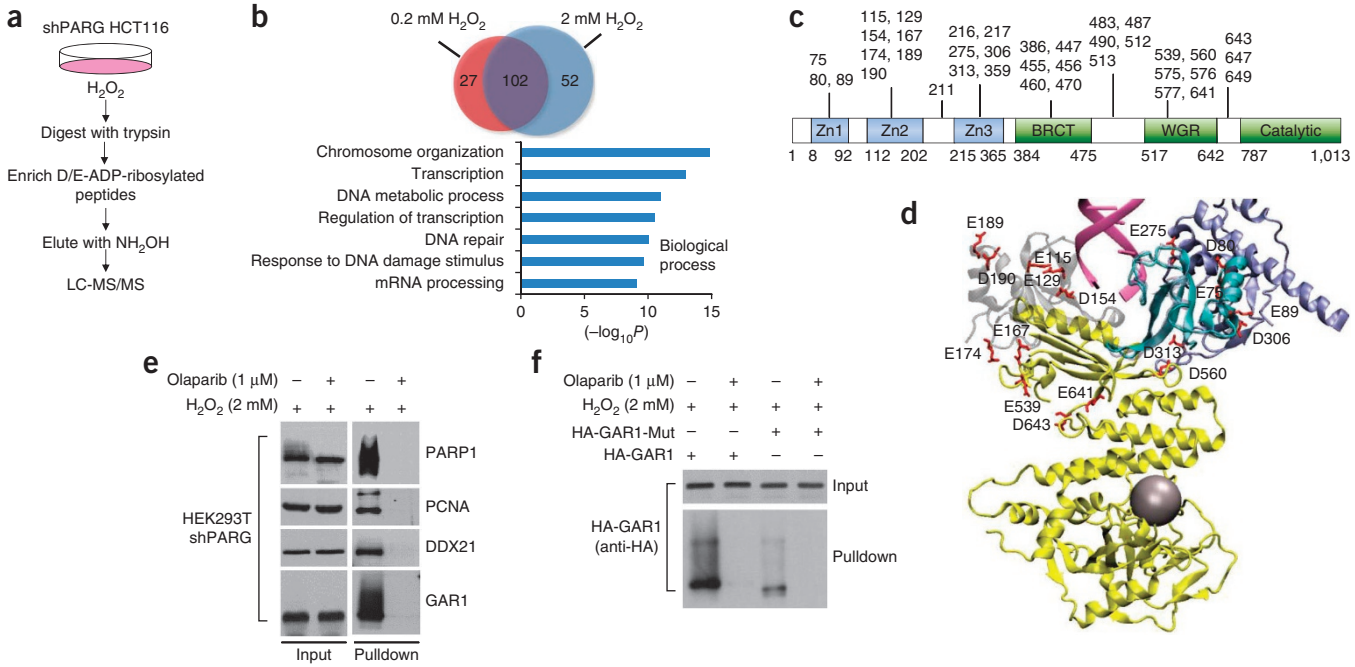

Figure 2 | Qualitative analysis of the human Asp- and Glu-ADP-ribosylated proteome. (**a**) Flowchart for the experimental procedure. (**b**) Asp- and Glu-ADP-ribosylated proteins identified in PARG-knockdown HCT116 cells treated with 0.2 mM and 2 mM H_2O_2, respectively. Biological processes enriched in the modified proteins are shown (hits from both experiments were combined for this analysis). (**c**) Unambiguously identified Asp- and Glu-ADP-ribosylation sites on PARP1. Data are combined from all qualitative and quantitative experiments. (**d**) Auto-modification sites (red) on PARP1. Residues 8–40 of the zinc finger 1 (Zn1) domain from two structures of PARP1 in complex with DNA[14,19] (PDB 4DQY; 4AV1) were used to align both structures to generate an overlaid presentation. For the former (PDB 4DQY), Zn1 is shown in cyan; Zn3 is shown in blue; WGR-catalytic domain shown in yellow. For the latter (PDB 4AV1), Zn1 and Zn2 are shown in gray; DNA is shown in magenta. The NAD^+ binding site is shown as a silver sphere. (**e**) Validation of the identified PARylated proteins. Input (whole cell lysates) and boronate-pulldown proteins were probed with anti-PARP1, anti-PCNA or anti-HA (to detect transfected DDX21 and GAR1). (**f**) PARG-knockdown HEK293T cells were transfected with wild-type (HA-GAR1) or mutant HA-GAR1 (HA-GAR1-Mut; E67Q, E74Q, E80Q, D81N and E104Q). Input and boronate-pulldown proteins were probed with anti-HA.

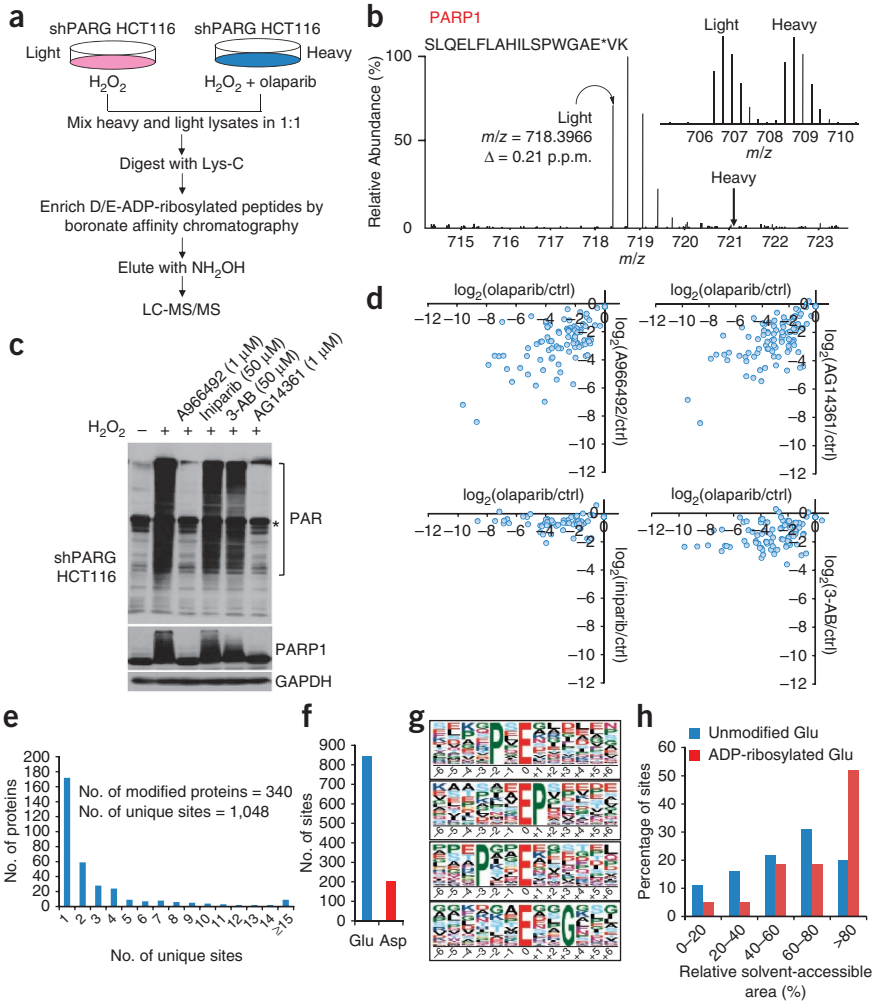

Figure 3 | Quantitative analysis of the human Asp- and Glu-ADP-ribosylated proteome. (**a**) Flowchart of the experimental procedure to characterize the ADP-ribosylated proteome upon PARP inhibition. (**b**) Identification of an olaparib-sensitive PARP1 auto-modified peptide. The heavy peptide was derived from the olaparib-treated cells, whereas the light peptide was from the untreated cells (both the light and heavy cells were then stimulated with H_2O_2). The site of modification is indicated by an asterisk. The inset shows a ~1:1 ratio (heavy/light) of a non-PARylated peptide (AELGIPLEEVPPEEINYLTRIHYK) from IPP isomerase. (**c**) Immunoblot analysis of PARylation after treatment with various PARP inhibitors. Whole-cell lysates were probed with the indicated antibodies. The asterisk indicates a nonspecific band. (**d**) Analysis of four PARP inhibitors (experimental procedure as in **a**) and their correlation with olaparib. Plots of $\log_2$(compound/control) values (or median values if identified multiple times) of the intensity of ADP-ribosylated peptides identified using olaparib and A966492, AG14361, iniparib or 3-AB. Only peptides with all modification sites confidently localized (MOD score ≥13) are included. Ctrl, control. (**e**) Distribution of the number of ADP-ribosylation sites per protein. (**f**) Distribution of ADP-ribosylation sites between aspartic acid and glutamic acid resides. (**g**) Motif analysis of Glu-ADP-ribosylation. (**h**) Compared to unmodified glutamic acid, ADP-ribosylated glutamic acid residues possess a larger solvent-accessible area. For **e**–**h**, data were combined from all qualitative and quantitative experiments.

($P = 1.33 \times 10^{-13}$), DNA metabolic process ($P = 1.03 \times 10^{-11}$) and DNA repair ($P = 1.01 \times 10^{-10}$) (modified Fisher's exact test) (**Fig. 2b** and **Supplementary Results**). We also applied the method to characterize Asp- and Glu-ADP-ribosylation after MNNG treatment (**Supplementary Results**).

Fragmentation of the NH_2OH-derivatized peptides yielded typical *b*- and *y*-ion series, allowing easy localization of the ADP-ribosylation sites (**Supplementary Fig. 3a**–**d**). The generation of a PARP1 mutant that catalyzed mono(ADP-ribosyl)ation was reported to lead to PARP1 auto-modification sites that mapped to Asp386, Glu487 and Glu490. However, mutation of these residues did not change the PARylation level of the full-length protein, indicating the presence of additional modification sites[10]. More recently, experiments using phosphodiesterase treatment and phosphopeptide enrichment identified 12 ADP-ribosylation sites on PARP1, and most of these sites localized to aspartic acid and glutamic acid residues[13]. We found that, *in vivo*, PARP1 was auto-modified with a total of 37 unambiguously assigned Asp- and Glu-ADP-ribosylation sites (**Fig. 2c**). Many of these sites and their flanking sequences are conserved evolutionarily and could be functionally relevant (**Supplementary Fig. 3b**). Mapping of the identified sites onto the structure of PARP1 favors the model that PARP1 might be auto-modified in *trans*[14] (**Fig. 2d** and **Supplementary Results**). We verified several ADP-ribosylated proteins, including proliferating cell nuclear antigen (PCNA), DEAD box protein 21 (DDX21) and H/ACA ribonucleoprotein complex subunit 1 (GAR1), by a combination of boronate pulldown and immunoblot assays (**Fig. 2e**). In addition, GAR1 was modified by PARP1 *in vitro*, and mutation of the identified ADP-ribosylation sites on GAR1 led to a greatly reduced level of PARylation both *in vitro* and *in vivo* (**Fig. 2f** and **Supplementary Fig. 3e**).

We performed stable isotope labeling by amino acids in cell culture (SILAC) experiments[15] to profile PARylation after PARP inhibitor treatment. Using single heavy lysine labeling, we observed a dramatic change in the ADP-ribosylated proteome after olaparib treatment (**Fig. 3a**, **Supplementary Fig. 4** and **Supplementary Table 3**), with a decrease of >50% in the intensities of >81% of modified peptides (**Supplementary Fig. 4a**). We repeated the experiment using heavy lysine and arginine double labeling and obtained a similar finding (**Supplementary Table 4**). Many Asp- and Glu-ADP-ribosylation sites were extremely olaparib sensitive. For example, the abundance of the PARP1 auto-modified peptide SLQELFLAHILSPWGAE*VK (E* indicates the site of ADP-ribosylation) decreased by more than 99% after olaparib treatment (**Fig. 3b**). In another example, ADP-ribosylation of two evolutionarily conserved glutamic acid residues on PCNA also dramatically decreased (**Supplementary Fig. 4c**–**f**). ADP-ribosylation of the tankyrase substrates CASC3 and BLZF1 (ref. 16), however, showed little change after olaparib treatment

(**Supplementary Table 3**), in agreement with the finding that olaparib is not a potent inhibitor of tankyrase[2].

We characterized the response of the Asp- and Glu-ADP-ribosylated proteome to four additional PARP inhibitors — A966492, AG14361, iniparib and 3-aminobenzamide (3-AB) (**Fig. 3c**, **Supplementary Fig. 1d** and **Supplementary Tables 5–8**). Mass spectrometric analyses showed that the change in protein ADP-ribosylation upon the treatment with A966492 or AG14361 correlated well with that of olaparib (**Fig. 3d**). In contrast, even at 50 μM, iniparib, a compound under clinical investigation for treatment of various cancers in humans, had little effect on H_2O_2-induced hyper-PARylation (**Fig. 3c**), in agreement with two recent studies that challenged the status of iniparib as a genuine PARP inhibitor[17,18]. Our mass spectrometric results further showed that, although the abundance of an ADP-ribosylated peptide from DDX21 (NEEPSE*EEIDAPKPK, **Supplementary Table 7**) decreased by ~80% upon iniparib (50 μM) treatment, most of the peptides had a change in ADP-ribosylation level of <50% (**Fig. 3d**), indicating that iniparib has a negligible effect on PARP activity in intact cells (**Supplementary Results**).

In total, we identified 1,048 unique, unambiguously localized Asp- and Glu-ADP-ribosylation sites on 340 proteins (**Fig. 3e** and **Supplementary Tables 1–13**). The ADP-ribosylated proteins had high network connectivity, with several of the clusters containing known macromolecular complexes (**Supplementary Figs. 5** and **6**). ADP-ribosylation occurred predominantly on glutamic acid residues, which represented more than 80% of the sites (**Fig. 3f**). Examination of a 6-aa window adjacent to modified glutamic acid residues revealed several consensus motifs ($P < 0.001$; binomial test), such as PXE*, E*P, PXXE* and E*XXG (**Fig. 3g** and **Supplementary Fig. 4b**). ADP-ribosylated glutamic acid residues had a marked tendency to reside on protein surfaces (**Fig. 3h** and **Supplementary Results**), indicating that solvent accessibility may be an important determining factor for whether a residue is modified.

In summary, we have identified many previously uncharacterized Asp- and Glu-ADP-ribosylated proteins involved in a wide array of nuclear functions. A large fraction of these proteins were downstream of PARP whose ADP-ribosylation ability was sensitive to the treatment of PARP inhibitors. We expect that the identified PARP targets will seed the future functional study of this important class of enzymes.

METHODS

Methods and any associated references are available in the online version of the paper.

Note: Any Supplementary Information and Source Data files are available in the online version of the paper.

ACKNOWLEDGMENTS

We thank S. McKnight and H. Yu for discussions. We thank H. Yu, H. Mirzaei and S. Gygi for access to the tissue culture, mass spectrometry and computation facilities, respectively. pCMV-Sport6-GAR1 and pCMV-Sport6-DDX21 were kind gifts from L. Lum (University of Texas Southwestern Medical Center). This work was supported by grants from the UT Southwestern Medical Center Endowed Scholar Program, the Cancer Prevention and Research Institute of Texas (CPRIT R1103) and the Welch Foundation (I-1800) to Y.Y. Y.Y. is a Virginia Murchison Linthicum Scholar in Medical Research and a CPRIT Scholar in Cancer Research.

AUTHOR CONTRIBUTIONS

Y.Y. conceived the project and designed the approach. Y.Y., Y.Z. and M.D. performed research and analyzed data. Y.Y. and J.W. performed computational analyses. Y.Y. supervised the project. Y.Y. wrote the manuscript with input from all coauthors.

COMPETING FINANCIAL INTERESTS

The authors declare competing financial interests: details are available in the online version of the paper.

1. Chambon, P., Weill, J.D. & Mandel, P. *Biochem. Biophys. Res. Commun.* **11**, 39–43 (1963).
2. Rouleau, M., Patel, A., Hendzel, M.J., Kaufmann, S.H. & Poirier, G.G. *Nat. Rev. Cancer* **10**, 293–301 (2010).
3. Krishnakumar, R. & Kraus, W.L. *Mol. Cell* **39**, 8–24 (2010).
4. Wahlberg, E. *et al. Nat. Biotechnol.* **30**, 283–288 (2012).
5. Farmer, H. *et al. Nature* **434**, 917–921 (2005).
6. Tulin, A. *Nat. Biotechnol.* **29**, 1078–1079 (2011).
7. Dani, N. *et al. Proc. Natl. Acad. Sci. USA* **106**, 4243–4248 (2009).
8. Hengel, S.M. & Goodlett, D.R. *Int. J. Mass Spectrom.* **312**, 114–121 (2012).
9. Hassa, P.O., Haenni, S.S., Elser, M. & Hottiger, M.O. *Microbiol. Mol. Biol. Rev.* **70**, 789–829 (2006).
10. Tao, Z., Gao, P. & Liu, H.W. *J. Am. Chem. Soc.* **131**, 14258–14260 (2009).
11. Liu, X.C. & Scouten, W.H. *Methods Mol. Biol.* **147**, 119–128 (2000).
12. Moss, J., Yost, D.A. & Stanley, S.J. *J. Biol. Chem.* **258**, 6466–6470 (1983).
13. Chapman, J.D., Gagne, J.P., Poirier, G.G. & Goodlett, D.R. *J. Proteome Res.* **12**, 1868–1880 (2013).
14. Ali, A.A. *et al. Nat. Struct. Mol. Biol.* **19**, 685–692 (2012).
15. Yu, Y. *et al. Science* **332**, 1322–1326 (2011).
16. Zhang, Y. *et al. Nat. Cell Biol.* **13**, 623–629 (2011).
17. Liu, X. *et al. Clin. Cancer Res.* **18**, 510–523 (2012).
18. Patel, A.G., De Lorenzo, S.B., Flatten, K.S., Poirier, G.G. & Kaufmann, S.H. *Clin. Cancer Res.* **18**, 1655–1662 (2012).
19. Langelier, M.F., Planck, J.L., Roy, S. & Pascal, J.M. *Science* **336**, 728–732 (2012).

ONLINE METHODS

Cells and reagents. HCT116 and HEK293T cells were purchased from ATCC and were maintained in Dulbecco's modified Eagle's medium (DMEM) supplemented with 10% FBS. PARP inhibitors were purchased from Selleck. Anti-poly-(ADP-ribose) monoclonal antibody was purchased from Trevigen (4335-MC-100, diluted at 1:1,000). Anti-HA antibody was purchased from Cell Signaling Technology (CST #3724, diluted at 1:1,000). PARP1 antibody was purchased from Cell Signaling Technology (CST #9532, diluted at 1:1,000). GAPDH antibody was purchased from Cell Signaling Technology (CST #5174, diluted at 1:1,000). Other chemicals and reagents were obtained from Sigma unless otherwise indicated.

Mammalian lentiviral short hairpin RNAs. Generation of the lentiviruses was carried out as described previously[15]. Briefly, an shPARG plasmid (Sigma, NM_003631.1-2843s1c1) was co-transfected into HEK293TD cells along with packaging (Δ8.9) and envelope (VSVG) expression plasmids using Lipofectamine 2000 (Invitrogen). Two days after transfection, viral supernatants were harvested and filtered. Recipient cells were infected in the presence of a serum-containing medium supplemented with 8 μg/ml polybrene. Following infection for 36 h, cells were treated with 2.0 μg/ml puromycin for 48 h to select cells that stably expressed the shPARG construct. PARG knockdown was confirmed by immunoblotting assays using an anti-PARG antibody (Millipore, MABS61, diluted at 1:1,000).

Boronate beads pulldown analysis. DDX21 and GAR1 were cloned into a pKH3 vector. The GAR1 point mutants (E67Q, E74Q, E80Q, D81N and E104Q) were generated using the QuickChange site-directed mutagenesis kit (Stratagene). PARG-knockdown HEK293T cells were transfected with the corresponding constructs using Lipofectamine 2000 (Invitrogen). Isolation of poly(ADP-ribosyl)ated proteins for immunoblotting analyses was performed as described[20] with modifications. Briefly, cells were lysed in SDS lysis buffer (1% SDS, 10 mM HEPES (pH 7.0), 2 mM $MgCl_2$, 500 U Benzonase), which were adjusted to pH 8.5. Lysates were mixed with *m*-aminophenyl-boronic acid–agarose. After 1 h incubation at room temperature, beads were washed with the SDS wash buffer (1% SDS, 100 mM HEPES (pH 8.5), 150 mM NaCl) and subsequently with the wash buffer (100 mM HEPES (pH 8.5), 150 mM NaCl). Beads were mixed with ammonium acetate (3 M, pH 5.0) for 1.5 h, and washed once with the SDS lysis buffer. Beads were incubated with 4× SDS-PAGE sample loading buffer at 95 °C for 10 min and the eluates were subjected to immunoblotting analyses.

SILAC cell culture. Cells (HCT116 shPARG) were grown in the SILAC medium as described previously[15]. Both light and heavy DMEM were supplemented with 10% dialyzed FBS (Invitrogen). Where indicated, cells were pretreated with 1 μM olaparib for 40 min and were stimulated with 2 mM H_2O_2 for 5 min. We performed two experiments using this experimental design with single labeling with lysine (sample digested with Lys-C) or double labeling with lysine and arginine (sample digested with trypsin). Each experiment was composed of two technical replicate analyses. Data for experiment 1 (single lysine labeling) were presented in **Figure 3** and **Supplementary Figure 4** for the purpose of illustration. The same experiment (lysine labeling only) was repeated for four other PARP inhibitors, including A966492 (1 μM), AG14361 (1 μM), iniparib (50 μM) and 3-AB (50 μM).

Sample preparation for mass spectrometric analysis. Cells were lysed in the SDS lysis buffer (1% SDS, 10 mM HEPES (pH 7.0), 2 mM $MgCl_2$, 500 U Benzonase). Lysates (25 mg for each experiment) were washed with the SDS lysis buffer for three times using Centricon ultrafiltration units (MWCO = 10,000 Da, Millipore), and were collected in the same buffer. Lysates were reduced by adding DTT to a final concentration of 3 mM, followed by incubation at room temperature for 20 min. Cysteines were alkylated by adding iodoacetamide to a final concentration of 50 mM, followed by incubation in the dark for 20 min. Lysates were digested with Lys-C or trypsin at a 1:100 (enzyme/substrate) ratio for 2 h at room temperature (RT) in the SDS lysis buffer.

m-aminophenylboronic acid–agarose (Sigma) beads were equilibrated by washing the beads three times using the buffer (1% SDS, 100 mM HEPES (pH 8.5)). pH of the lysates was adjusted to 8.5 and the lysates were incubated with these beads for 1 h at RT. Beads were washed with the SDS wash buffer (1% SDS, 100 mM HEPES (pH 8.5), 150 mM NaCl) for three times, and then the wash buffer (100 mM HEPES (pH 8.5), 150 mM NaCl) for five times. Peptides were eluted by incubating the beads with 0.5 M NH_2OH overnight at RT on an end-to-end rotator. Released peptides were desalted on SepPak C18 columns (Waters) according to the manufacturer's instructions.

Mass spectrometry analysis and data processing. Samples were analyzed by LC-MS/MS on an LTQ-Velos Pro Orbitrap mass spectrometer (Thermo Fischer Scientific, San Jose, CA) using a top20 method[21]. The isolation window and the minimal signal threshold for MS/MS experiments were set to be 2 Th and 500 counts, respectively. The ReAdW.exe program was used to convert the raw files into the mzXML format[22] (http://sashimi.svn.sourceforge.net/viewvc/sashimi/). MS/MS spectra were searched against a composite database of the human IPI protein database and its reversed complement using the Sequest algorithm. Search parameters allowed for a static modification of 57.02146 Da on cysteine and a dynamic modification of addition of 15.0109 Da to aspartic acid and glutamic acid, and, when applicable, the stable isotope (10.00827 Da and 8.01420 Da) on arginine and lysine, respectively. Search results were filtered to include <1% matches to the reverse database by the linear discriminator function using parameters including Xcorr, dCN, missed cleavage, charge state (exclude 1+ peptides), mass accuracy, peptide length and fraction of ions matched to MS/MS spectra[22]. Localization of ADP-ribosylation sites was assessed by the ModScore algorithm based on the observation of site-specific fragment ions[23]. Sites with scores ≥13 ($P \leq 0.05$) were considered localized. Peptide quantification was performed as previously described[15]. ADP-ribosylation motifs were extracted using the Motif-X algorithm[24] with a significance threshold of $P < 0.001$.

***In vitro* PARylation reaction.** HEK293T cells were transfected with HA-GAR1 or HA-GAR1 mutant (E67Q, E74Q, E80Q, D81N and E104Q). Before lysis (sonication 10%, 5 s per cycle, five total cycles), cells were treated with olaparib (3 μM) for 40 min. Olaparib (3 μM) was also included in the lysis buffer A (40 mM

HEPES, pH 7.5, 120 mM NaCl, 1 mM EDTA, 1% Triton X-100 and 1% NP40 with a protease/phosphatase inhibitor cocktail) to prevent the artificial activation of PARP1, as a result of sonication-induced DNA fragmentation. Proteins were immunoprecipitated with anti-HA beads. The beads were washed and were incubated (RT, 1hr) with PARP1 (500 ng, Tulip Biosciences) and NAD^+ (500 μM) in the reaction buffer (50 mM Tris, pH 7.5, 4 mM $MgCl_2$, 20 mM NaCl and 250 μM DTT with 100 ng sheared salmon DNA added to each reaction). When indicated, olaparib (3 μM) was added to block the *in vitro* PARylation reaction. Reactions were terminated by SDS loading buffer and were probed by an anti-HA antibody.

***In vitro* PARG treatment.** One microgram of auto-modified PARP1 (Tulip) was treated with 30 ng PARG (Trevigen) in the reaction buffer (50 mM K_3PO_4, 50 mM KCl, pH 7.5) for 1 h at 37 °C. The pH of the solution was adjusted to 8.5, which was subsequently loaded onto the boronate beads. The flow-through as well as the eluted fractions (using NH_4OAc) were analyzed by immunoblotting assays.

Immunoblotting analysis. Samples were subjected to electrophoresis using the standard SDS-PAGE method. Proteins were transferred to a nitrocellulose membrane (Whatman). Membranes were blocked with a TBST buffer (25 mM Tris-HCl, pH 7.5, 150 mM NaCl, 0.05% Tween 20 and 3% nonfat dried milk), and probed overnight with primary antibodies at 4 °C and with peroxidase-conjugated secondary antibodies for 1 h at RT. Blots were developed using enhanced chemiluminescence, exposed on autoradiograph film and developed using standard methods.

Calculation of the relative solvent-accessible area. Twenty-five structure files were found in the Protein Data Bank (PDB) that corresponded to proteins that contained multiple ADP-ribosylation sites, including LIG3 (1UW0, 1IMO), EWS (2CPE), PCNA (1VYM), FBL (2IPX), FEN1 (3q8k), SERPINC1 (2B4X), H2AFY (3IID), UBC (1aar), NCL (2FC9), GAPDH (1U8F), LDHB (1T2F), H2AFY2 (2XD7), FUS (2LA6), THOC4 (3ULH), TOP1 (1A31), PARP1 (2L30, 2L31, 2RIQ, 2COK, 2CR9), UHRF1 (3CLZ), MKI67 (1R21), UBTF (1K99) and YY1 (1UBD). Singly modified proteins were excluded to minimize the bias introduced by unidentified ADP-ribosylation sites in the proteins. Unambiguously localized ADP-ribosylated glutamic acid residues (a total of 59 sites) were mapped onto the structures and the relative solvent-accessible side-chain area for ADP-ribosylated and unmodified glutamic acid residues was calculated by NACCESS[25] with a default probe size of 1.4 Å.

20. Oei, S.L. & Shi, Y. *Biochem. Biophys. Res. Commun.* **285**, 27–31 (2001).
21. Olsen, J.V. *et al. Mol. Cell. Proteomics* **8**, 2759–2769 (2009).
22. Huttlin, E.L. *et al. Cell* **143**, 1174–1189 (2010).
23. Kim, W. *et al. Mol. Cell* **44**, 325–340 (2011).
24. Schwartz, D. & Gygi, S.P. *Nat. Biotechnol.* **23**, 1391–1398 (2005).
25. Hubbard, S.J., Campbell, S.F. & Thornton, J.M. *J. Mol. Biol.* **220**, 507–530 (1991).

doi:10.1038/nmeth.2603

Erratum: Site-specific characterization of the Asp- and Glu-ADP-ribosylated proteome

Yajie Zhang, Jianqi Wang, Ming Ding & Yonghao Yu
Nat. Methods; **doi:10.1038/nmeth.2603; corrected online 26 August 2013**

In the version of this article initially published online, the *x*-axis tick label "≥15" in Figure 3e was mislabeled. The error has been corrected for the print, PDF and HTML versions of this article.